*Renewable Energies Offshore – Guedes Soares (Ed.)*
*© 2015 Taylor & Francis Group, London, ISBN: 978-1-138-02871-5*

# Experimental loss analysis on a model-scale radial bidirectional air-turbine for wave energy conversion

C. Moisel & T.H. Carolus
*Institut für Fluid und Thermodynamik, University of Siegen, Germany*

ABSTRACT: A wide variety of bidirectional turbine concepts to equip oscillating water column (OWC) wave energy converter have been proposed over the last decades. Objective of this study is a detailed experimental investigation of a radial bidirectional lift-based air-turbine and comparison to numerically predicted performance characteristics. The turbine concept, first suggested by Kentfield (1983) has never been investigated experimentally until today. The new bi-directional aero-acoustic turbine test rig at the University of Siegen, Germany is employed to determine experimental aerodynamic performance characteristics of the radial turbine. Particular emphasis is placed on a detailed analysis of the turbines internal losses: rotor disc friction and leakage. The experimental results are utilized to compare to numerically (RANS) predicted characteristics. It was found that especially the rotor skin friction loss has a remarkable influence on the radial turbines performance. General findings derived could provide guidelines for further development of the turbines conceptual design and investigation process.

## 1 INTRODUCTION

Over the last decades oscillating water column (OWC) wave energy converter have been studied extensively, see e.g. Cruz (2008) and Falcão (2010). The wave collector transforms ocean surface motions into and oscillatory pneumatic power (pressure/flow rate). By employing a bidirectional air-turbine, a rectified torque can be generated to drive an electric generator. A wide variety of different turbine concepts have been presented capable to equip an OWC wave power plant, see e.g. Setoguchi & Takao (2006), Curran & Folley (2008), Falcão & Gato (2012). One of these concepts is the radial bidirectional lift-based turbine, suggested by Kentfield (1983), but however has not been much under investigation until today. Numerical investigations of the turbines radial lift-based cascade carried by Moisel & Carolus (2013, (2014) have shown its operational characteristics. A study by Moisel & Starzmann (2013) introduced a turbine design methodology based the blade element momentum method (BEM) and presented first numerically predicted performance characteristics of a full turbine setup with an optimized axial/radial meridional contour, including a set of axial guide vanes.

In this study we present first experimental results of the radial lift-based turbine (rotor diameter $D = 0.4$ m), measured on the new bidirectional steady-state aero-acoustic test facility at University of Siegen, Germany. A detailed experimental investigation of the turbines disc friction and leakage losses is carried out to get a further understanding on its effects and improvement potential. Finally the experimental results 'corrected' by the loss issues, not modelled within the numerical domain, are compared to the numerically (RANS) predicted results.

## 2 RADIAL TURBINE DESIGN

### 2.1 *Radial turbine concept*

In the 1980ies a lift-based turbine with a *radial* cascade of non-staggered blades has been proposed by Kentfield (1983). Fig. 1 pictures a 3D-model of the numerically optimized radial turbine design proposed by Moisel & Starzmann (2013) with radial rotor blades and a set of axial guide vanes. The flow either enters the rotor axially or leaves it in radial direction (centrifugal flow direction) or vice versa (centripetal flow direction).

An outstretched hub cone assists the flow turning direction between axial and radial sections and prevents hub dead water zones when the flow enters the axial section downstream of the rotor in centripetal direction.

### 2.2 *Rotor layout and cascade parameters*

The rotor blades are fundamentally built from symmetrical 4-digit NACA series airfoils. In contrast to an axial blade, each segment of a radial rotor blade is located on the same radius, i.e. it moves with the same circumferential velocity. This avoids any needs for blade twisting and hence has the potential of increased peak efficiency, extended stall free operational range

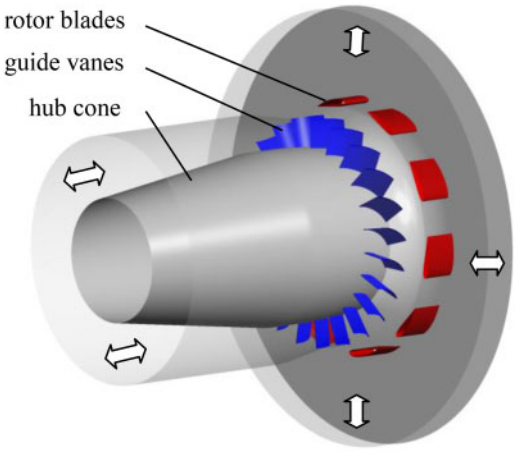


Figure 1. Radial turbine – 3D model.

and less noise emission due to partial flow separation compared to the Wells turbine. To incorporate for the radial flow field, the blades are mapped geometrically on the impellers radius. The 'conformal mapping' method based on potential flow theory was introduced for the radial turbine by Moisel & Carolus (2013).

In earlier studies for the radial lift-based turbine cascade it was found by Moisel & Carolus (2014) that 3D side wall/blade surface boundary layer interactions have a considerable influence on the rotor blade efficiency and overload capacities. Hence the blade section is designed with some side wall contouring inside of the impellers mean line to reduce the side wall boundary layer effects.

Throughout this study we describe the mixed-flow turbine cascade with certain non-dimensional parameters:

The solidity

$$\sigma \equiv \frac{L}{t} \tag{1}$$

with $L$ = chord length and $t$ = circumferential blade spacing defined as

$$t = \frac{\pi D}{z} \tag{2}$$

where $z$ = number of blades,

The relationship of $b$ = blade width to D = diameter

$$\upsilon_r = \frac{b}{D}, \tag{3}$$

the aspect ratio

$$AR \equiv \frac{L}{b}, \tag{4}$$

the Reynolds number

$$Re_L \equiv \frac{Lu}{\nu} \tag{5}$$

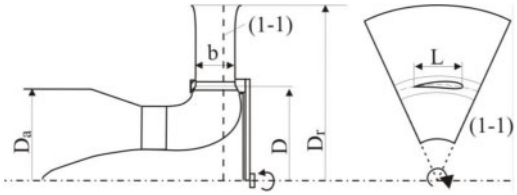


Figure 2. Mixed flow turbine – main geometric parameters.

Table 1. Main parameter of the investigated turbine.

| Parameter | Unit | Value |
|---|---|---|
| D | m | 0.40 |
| $D_r$ | m | 1.75 · D |
| $D_a$ | m | 1.0 · D |
| $s_{1-3}$/D | – | 0.001 |
| z | – | 9 |
| $\upsilon_r$ | – | 0.14 |
| AR | – | 1.4 |
| $\sigma$ | – | 0.56 |
| Airfoil | – | NACA 0015 |
| n | rpm | 4000 |
| Ma | – | 0.24 |
| $Re_L$ | – | 4.3e5 |

with $u_D$ = rotational velocity at nominal turbine diameter and $\nu$ = kinematic viscosity, and the Mach number

$$Ma_u \equiv \frac{u}{a} \tag{6}$$

where $a$ = speed of sound.

Note that the relevant velocity for *Re* and *Ma* is the blades' rotational velocity $u$ which is – for cascades with small deflection – in the same order of magnitude as the relative flow velocity $w_\infty$ to the blades.

### 2.3 *Turbine dimensions*

The radial turbine layout with main geometric dimensions highlighted is displayed schematically in Figure 2.

The main geometric turbine dimensions and cascade parameter are compiled in Table 1.

Additionally to the variables and dimensions already introduced or indicated in Figure 2 the gap dimensions between rotor and ducting s are listed in relation to the rotors nominal diameter D.

### 2.4 *Aerodynamic coefficients and performance parameters*

The aerodynamic performance of lift-based OWC air-turbines is generally described by the pressure coefficient

$$\psi \equiv \Delta p \Big/ \left( \frac{\pi^2}{2} \rho D^2 n^2 \right) \tag{7}$$

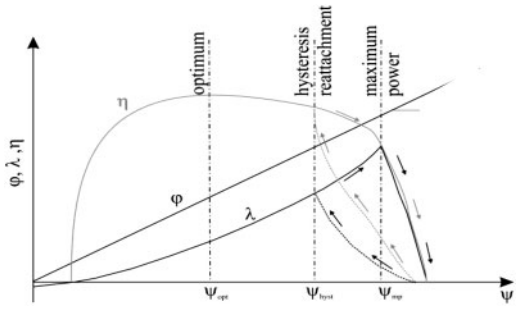


Figure 3. Lift-based turbines steady state characteristic curves (schematically).

where $\Delta p$ = pressure drop, $\rho$ = local density, $D$ = nominal rotor diameter and $n$ = rotational speed.

The flow rate coefficient

$$\phi \equiv \dot{V} \Big/ \left( \frac{\pi^2}{4} D^3 n \right) \tag{8}$$

with $\dot{V}$ = volume flow rate.

The power coefficient

$$\lambda \equiv T\,\omega \Big/ \left( \frac{\pi^4}{8} \rho D^5 n^3 \right) \tag{9}$$

where $T$ = torque and $\omega$ the angular velocity.

Finally the efficiency can be derived by the ratio of power coefficient and pneumatic power available represented by flow rate and pressure coefficient

$$\eta = \lambda / \phi\psi\,. \tag{10}$$

Depending on the implemented control strategy turbines in OWC application are operated along its complete characteristic curve from no load via optimum operation to overload, maybe even into deep stall, and back. A complete set of aerodynamic steady-state characteristic curves of bidirectional lift-based turbines, including a hysteresis loop after deep stall conditions, are displayed schematically in Figure 3.

Due to the bidirectional flow through the turbine in an OWC system, the magnitude of the hysteresis loop occurring after a stall event should be small to achieve maximum average power conversion in an OWC system. Therefore besides the optimum operating point at peak efficiency and the operational range, the turbine hysteresis ratio

$$h = \psi_{mp} / \psi_{hyt} \tag{11}$$

defined as $\psi_{mp}$ = pressure coefficient at maximum power dividend by $\psi_{hyst}$ = pressure coefficient at reattaching point after hysteresis may play an important role.

## 3 NUMERICAL SETUP

The flow in the radial lift-based turbine is simulated using the commercial 3D Navier-Stokes code

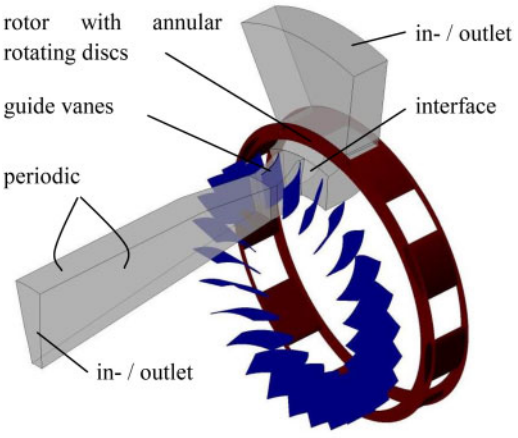


Figure 4. Numerical domain.

ANSYS CFX™ with the standard SST-turbulence-model Menter (1994) and the 'high resolution advection scheme' ANSYS (2013). The rotor diameter of 0.4 m was realized the same as for the experiments and a rotational speed of 4000 rpm chosen. In the composite computational domain (Figure 4) the steady, incompressible, three-dimensional Reynolds-averaged Navier-Stokes (RANS) equations are solved in a rotating reference frame (in the section where the rotor is placed) and in a stationary reference frame (where the guide vane) is placed. The block-structured numerical grid, prepared employing ANSYS TurboGrid™ consists of about 2 million nodes. Common grid quality criteria were considered; for instance the grid angles are all above 34°. The maximum value of $y^+_{max}$ for the first node adjacent to the blade surface (of rotor and stator) was set in TurboGrid™ to $y^+ < 1$ at a Reynolds Number Re = 4.3e5, a suitable mesh resolution out of a mesh refinement study.

The rotating reference frame of the rotor section and the stationary reference frame of the guide vane section are linked by the common so called 'stage interface'. At this connection only the averaged fluxes are transformed from the upstream reference frame through the interface. Steady state solutions are then obtained in each reference frame ANSYS (2013). Due to the turbine symmetry, only one blade annulus was modelled and 1:1 periodic boundary conditions were imposed in the circumferential direction. An inlet normal mass flow rate was imposed on the respective upstream boundary for each flow direction; an area averaged static pressure at the corresponding downstream boundary. Note that within this study there is no tip or duct clearance and no drive pulley modelled in the computational domain. Convergence was evaluated by monitoring the integral performance parameters, e.g. blade torque. For pre-stall points a mean deviation range of the blade torque monitor point below 1.5% had been achieved. Note that stall prediction is vague with a RANS approach, because of the

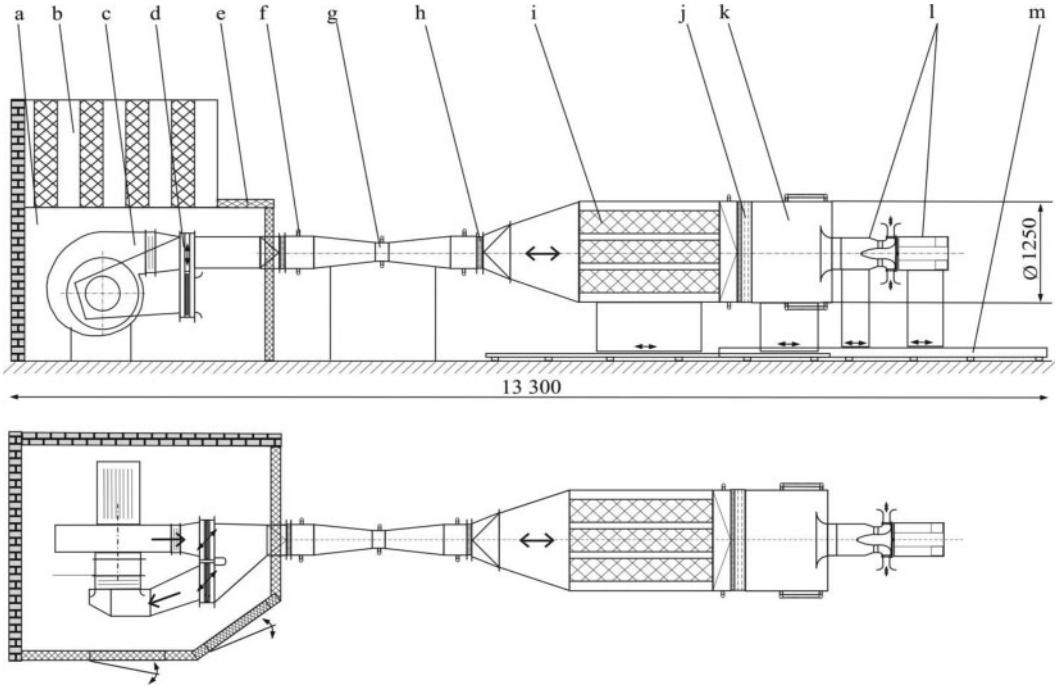


Figure 5. Bidirectional test facility – top: side view; bottom: top view: a) housing, b) splitter attenuator, c) centrifugal fan, d) flow diverter, e) acoustic housing, f) static pressure tapings, g) calibrated venturi nozzle, h) honeycombs, i) splitter attenuator, j) honeycombs and turbulence control screens, k) plenum, l) turbine section, m) linear track.

unsteady flow behavior and therefore the poor convergence in the turbine's overload operating regime. These post-stall operating points showed torque fluctuations exceeding 20%.

## 4 EXPERIMENTAL SETUP

### 4.1 *Hardware layout*

The layout of the new bidirectional steady-state test facility at University of Siegen is depicted in Figure 5. The variable but steady bi-directional volume flow rate in the facility is realized via a variable speed driven centrifugal fan (c), combined with a unique directional control valve (d) located in an acoustic enclosure (e), where the flow noise from inlet and outlet being controlled by acoustic absorbers (b, i). A symmetric venturi nozzle (g), accommodating honeycombs (h) on each side, is located between control valve and the acoustic absorber (i). A large plenum (k) contains screens and honeycombs (j) as flow straighteners for swirl and turbulence reduction. Model turbines can be mounted to the left side of the plenum chamber in the turbine section (l). The flexibly adjustable turbine basement is mounted on a linear track, allowing short setup times and precise positioning of the turbine components. Via the directional control valve, two operational modes can be realized within the test rig. The pressure side operation with positive pressure head between plenum and laboratory environment

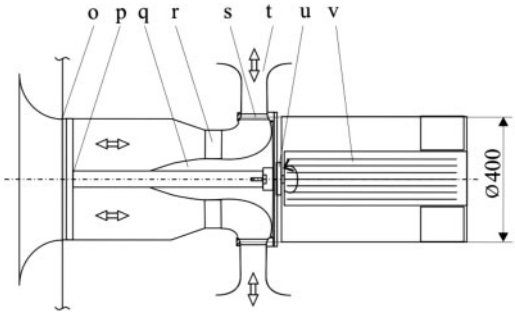


Figure 6. Radial Turbine – experimental setup: o) axial cylindrical duct connection to the plenum, p) hub cone support structure, q) outstretched hub cone, r) guide vanes, s) radial rotor, t) radial flow channel, u) generator.

and hence flow direction from the plenum into the turbine section. In the suction side operation the pressure head between plenum and lab is negative so that the air is sucked via the turbine section into the plenum. A detailed schematic representation of the turbine section (l) with embedded radial turbine is given in Figure 6.

The turbine is connected via an axial cylindrical ducting (o) to the plenum chamber. By use of a support structure (p) the hub cone (q) and the guide vanes (r) are mounted into the axial flow channel. The rotor (s) of D = 400 mm is mounted via a telemetric torque flange (u) on the generator (v). The radial flow channel

outside of the rotor is open to the laboratory environment. Note that contrary to the numerical domain there are struts of the support structure (q) within the axial section of the turbine.

Furthermore the rotor blades and annular rings are mounted to a rotor disc, enabling the connection to the drive train.

### 4.2 *Sensors & data acquisition*

The test facilities measurement system allows data acquisition for pressure head, flow rate, density, turbine torque and speed as well as acoustic sound pressure and power. The pressure head is determined via static pressure tappings at the walls of the large plenum (i), where also the temperature of the air-flow is measured. Note that the position of the relevant pressure tapping's for the particular flow direction is defined downstream of the honeycombs and turbulence screens (j) to prevent swirl components to distort the static pressure signal. Bidirectional measurement of the volume flow rate is realized via a carefully calibrated symmetric venturi nozzle (g). Torque is measured via an integrated telemetric torque flange, connecting directly turbine rotor and generator shaft. An incremental rotary encoder mounted to the generator shaft measures the turbines rotational speed. A control and data acquisition system is used to collect instantaneous data for each point of operation.

### 4.3 *Test procedure and data analysis*

Aerodynamic and acoustic turbine tests are carried out under bidirectional steady sate conditions. The test procedure is as follows:

- The turbine rotor is kept at constant speed;
- Pressure in the plenum chamber and volume flow rate is increased incrementally from zero beyond turbine aerodynamic stall and back;
- Flow direction in the rig is inverted; afterwards same procedure as above.

Within the fully automated measurement process each incremental measurement point is adjusted and after a dead time of 2 seconds to allow fully stable conditions a measurement is taken for 2 seconds at a sample rate of 2000 Hz and the signal finally averaged. Within this study acoustic characteristics are not addressed.

### 4.4 *Loss analysis procedure*

#### 4.4.1 *Rotor disc losses*

One main issue especially known in the field of radial turbo machinery are friction losses on the rotor disc, see e.g. Dixon & Hall (2010). This effect is investigated for the radial turbine in detail. To separate the losses from rotor disc and the friction losses produced by the blade cascade, a setup is realized where the rotor disc is separated from the blades and its annular rings. In Figure 7 a schematic cut-out of the radial rotor setup

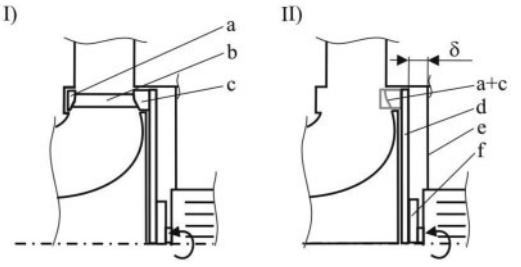


Figure 7. Radial Turbine – schematic sketch of the rotor plane in the experimental setup: I) original rotor setup, II) rotor disc friction loss setup: a) annular ring at shroud, b) blade cascade, c) annular ring at hub, d) rotor disc, e) plate f) telemetric torque flange, $\delta$) rotor to housing distance.

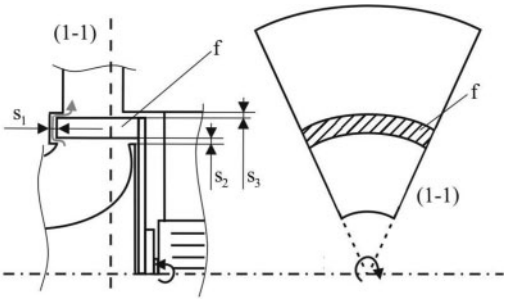


Figure 8. Radial Turbine – leakage loss setup: f) annular ring of solid material ('rotor dummy').

is pictured in I) and the modified setup for the disc friction tests in II).

The blade cascade (b) is removed and only the rotor disc (d) is left. Results of a setup including additionally the effect of the rotors annular rings ($a + c$) are determined analytically.

#### 4.4.2 *Leakage losses*

To determine the leakage losses within the experimental setup, preparations on turbine and the test facility's air supply are carried out. The schematic test setup of the turbines rotor section is pictured in Figure 8. The rotor blades and annular discs are replaced by solid cylindrical ring 'rotor dummy' (f), maintaining the same gap dimensions ($s_1$–$s_3$) between rotor and turbine housing. Note that only through the gap $s_1$ a leakage flow can be transported. The sections behind gap $s_2$ and $s_3$ are closed to the free environment; hence no leakage flow can leave. By disconnecting the test rigs plenum from the air supply between venturi nozzle (g) and splitter attenuator (i) in Figure 6, and inserting a solid plate at the connection, the plenum is sealed, with exception of the gaps between rotor and ducting of the turbine.

Employing the laboratory pressurized air-supply; air is transported into the plenum. The mass flow of the inserted air is measured employing a pipe mass flow meter while the plenum pressure is observed. Keeping the 'rotor dummy' spinning at its nominal rotational speed (4000 rpm), the particular mass flows

to keep a range of different plenum pressures constant is measured. The mass flow inserted to the chamber to maintain a constant pressure is than exactly the leakage flow leaving the rotor passage through the gaps. Note that leakage flows within the test rig setup were checked previously by sealing the plenum additionally at the connection to the turbine section and found to be negligible.

## 5 RESULTS

### 5.1 *Characteristic curves*

Fig. 9 shows steady state characteristic curves ($Re_L = 4.3e5$) from no load to stall, measured on the steady state test rig at University of Siegen. The volume flow-rate $\phi$, power coefficient $\lambda$ and the total to static efficiency $\eta_{ts}$ are plotted over the total to static pressure drop $\psi_{ts}$ for the centripetal (cpt) and centrifugal (cfg) flow direction. It appears at first glance that the $\phi/\psi$ characteristics of the radial turbine are nearly linear, as known for the Wells turbine. But obviously deviates the performance and the operational range between cfg and cpt direction. The operational range and power output is reduced for the cpt direction. As the radial turbine layout is for the flow under both flow directions not fully identical, it is possible but not desirable and wasn't expected in such extend through numerical investigations beforehand. A possible issue is that within the manufacturing process the surface properties of the inner side of the blades, acting as the (critical) suction side in cpt operational mode, were not finished as desired. One has to remanufacture the blades to see if this is the key issue for the differences detected. Note that the characteristic curves are plotted not including hysteresis loop because No visible differences were detectable between the performance before and after a turbine stall event (hysteresis ratio $h \approx 1$). Hence no hysteresis effect can be identified for the radial turbine, contrary as for the axial lift-based turbine (Wells turbine), see e.g. Starzmann, et al. (2011). Based on the numerical studies carried out beforehand (Moisel & Starzmann (2013)) one would have expected higher peak efficiencies in the experimental as $\eta_{ts,cfg,opt} \approx 65\%$ and $\eta_{ts,cfg,opt} \approx 60\%$. Hence an experimental loss analysis is carried out to understand more about possible issues in place within the experiment.

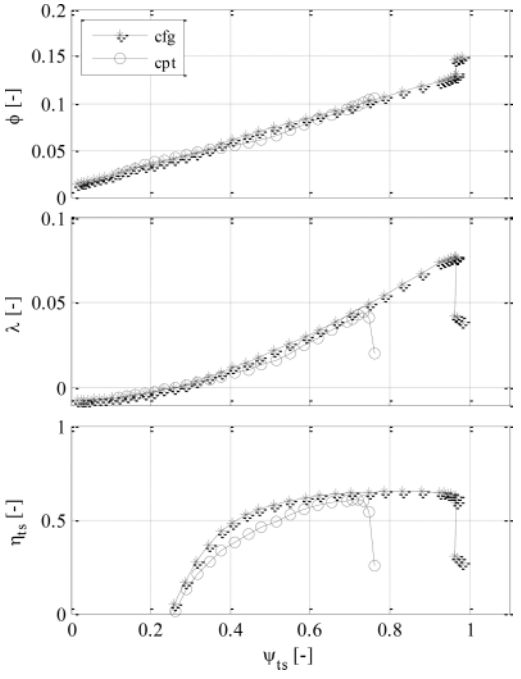


Figure 9. Measured aerodynamic steady state characteristic curves.

### 5.2 *Internal losses*

#### 5.2.1 *Rotor disc losses*

The frictional torque $T_f$ caused by a spinning plate is generally a function of

$$T_f = c_T \, \rho/2 \, \omega^2 \, R_{disc}^{\,5}. \tag{12}$$

whereupon the torque coefficient $c_T$ is a function of the Reynolds number $Re_R$ derived with the discs radius (in this study $R_{disc} = 0.209$) and the circumferential speed $u$, Sigloch (2009). In case of the turbine rotor disc two sides of the disc have to be considered and the installation situation incorporated. Due to boundary layer influences the flow resistance of the disc deviates noticeably between free or enclosed environment and the distances to the adjacent walls. Within an extensive experimental optimization process carried out by Horsthemke (2014) it was found that the best results could be achieved by inserting a plate (e) (Figure 7) at one side of the rotor disc. The optimal distance between blade and disc was found to $\delta/D_{disc} = 0.03$. Based on the findings of the study, one side of the rotor disc was considered as open where the flow could be transported radially outwards by the disc (side of the flow channel) and the other side as closed (side where the generator is located). Employing the torque coefficients based on Bohl (2008) for turbulent flow (Criteria $Re_R > 3 \times 10$) $c_{T,open} = 0.146/Re^{1/5}$ and $c_{T,enclosed} = 0.0622/Re^{1/5}$ the cumulated frictional torque could be derived. In this study the disc friction is displayed by the power coefficient $\lambda_f$ derived with the frictional torque and employing Equation 9. Depicted in Figure 10 are the results of the experimental investigation, generated by a variation in rotational speed. The analytical results based on Bohl (2008) are displayed as solid line.

Visible is that the analytical results fit well with the experimental data. Enabling a direct comparison of experimental and numerical results additionally to the rotor disc, the lateral surface friction of the blades annular rings have to be considered, as these are not modeled within the numerical domain. Therefore the

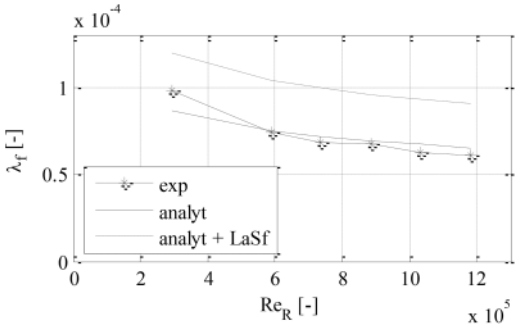


Figure 10. Rotor friction loss.

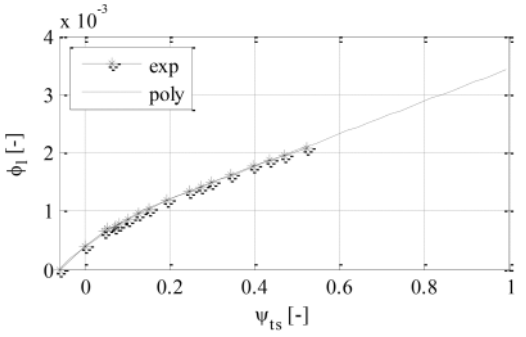


Figure 11. Leakage loss.

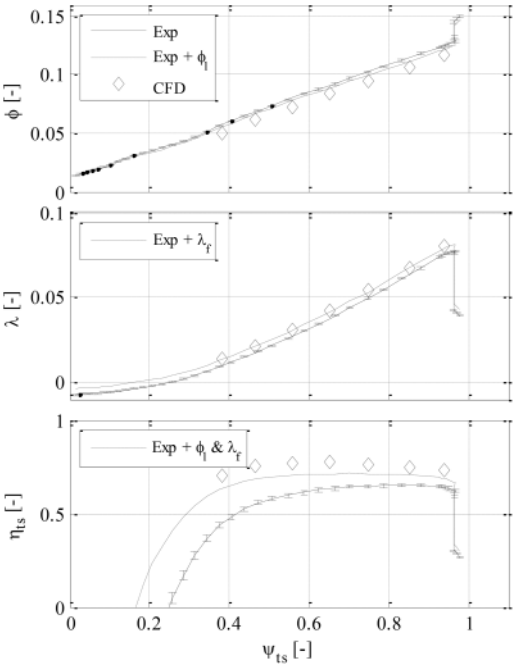


Figure 12. Characteristic curves; loss evaluation – cfg flow direction.

analytical model was extended to incorporate the lateral surfaces (LaSf) of (a + c) in Figure 7 and the results displayed as dashed line. A visible increase in friction loss can be detected.

5.2.2 *Leakage losses*

The results of the leakage loss measurements are depicted in Figure 11. The values are displayed by use of the 'leakage' flow rate coefficient $\phi_l$ and the total to static pressure coefficient $\psi_{ts}$ derived with the rotors nominal diameter D the rotational speed n = 4000 rpm, the leakage flow and the differential pressure between plenum and laboratory. Note that the measuring range of the available mass flow meter was limited to $\dot{m} = 1.5\,\mathrm{m^3/min}$. Hence, not the full range of relevant plenum pressures for the turbine setup could be determined.

The experimental results are displayed as the solid line with markers, whereupon a polynomial is used to extrapolate the values exceeding the measurable range. Mentionable is that the spinning disc generates a negative pressure in the plenum when no flow rate is transported into the plenum, hence acting as a 'bladeless' turbo machine.

5.2.3 *Effect of internal losses on performance characteristics*

In Figure 12 graphs of the flow rate coefficient, power coefficient and efficiency are plotted exemplary for the cfg direction. Experimental results including error bars indicate the measured characteristics including all losses and information about the uncertainty of the determined values. Visualized by the dashed lines are the experimental characteristics containing corrections of the respective influences of the disc friction and volumetric losses. Note that for the corrections of the disc friction the values of the analytical prediction including lateral surfaces (LaSf) was considered at $\mathrm{Re_D} = 1.18 \times 10^6$ (4000 rpm) to be able to realize an almost comparable configuration to the numerically predicted results, additionally depicted in the figure. Comparing the experimental results with and without internal loss correction it can be stated that especially in the power coefficient a remarkable increase in power can be detected when the disc friction losses are removed. Furthermore, this leads to a production of power at lower pressures as the negative 'burden' is reduced considerably. This results in wider operational range of high efficiencies and a difference in peak efficiency of about 5%. Die difference in peak efficiency due to leakage losses is estimated to about 2%. Comparing the results with the loss correction with the numerical results, still a difference between experimental and numerical data is detectable for the volume flow rate, whereupon the power coefficient is virtually identical. This finally yields still a difference in computed and measured efficiency.

This could be drawn back to struts within the mechanical setup in the experiment not being modelled in the numerical domain or divergences within the flow field which hasn't been investigated in detail until today.

## 6 CONCLUSIONS

A radial bidirectional lift-based turbine (rotor diameter of 0.4 m) has been investigated experimentally for the first time ever, employing the new bidirectional test facility at University of Siegen, Germany. Characteristic curves of the turbine design have been presented, and demonstrate the operability of the radial turbine concept. Nevertheless undesired divergences between centrifugal and centripetal flow direction have been identified but could most likely lead back to manufacturing issues of the rotor. An experimental loss analysis dealing with the measuring method and estimation of rotor disc friction and leakage losses on the turbines performance is carried out to study possible improvement potentials for the turbine concept. It is found that especially the rotors disc friction losses limit the achievable efficiency of the radial turbine remarkably. A comparison to numerically predicted results (RANS) yields some differences compared to the experimental results which should be investigated within further experimental investigations.

## ACKNOWLEDGMENTS

This work is sponsored by the German Federal Ministry for the Economics and Energy with the support code 0325396.

## REFERENCES

Ansys 2013, ANSYS CFX-Solver Modeling Guide, Release 14.5, ed. Canonsburg, Pennsylvania, 2013.

Bohl, W. 2008, *Technische Strömungslehre* vol. 14. Würzburg: Vogel Industrie und Medien GmbH & Co. KG.

Cruz, J. 2008, *Ocean Wave Energy: Current Status and Future Perspectives* Berlin: Springer-Verlag.

Curran, R. & Folley, M. 2008, Air turbine design for OWC's, in *Ocean Wave Energy: Current Status and Future Perspectives*, J. Cruz, Ed., ed Berlin: Springer-Verlag, 2008.

Dixon, S. L. & Hall, C. A. 2010, *Fluid Mechanics and Thermodynamics of Turbomachinery*, 6th ed. Boston: Butterworth Heinemann.

Falcão, A. F. D. O. 2010, Wave energy utilization: A review of the technologies, *Renewable and Sustainable Energy Reviews,* vol. 14, pp. 899–918.

Falcão, A. F. O. & Gato, L. M. C. 2012, Air Turbines, in *Comprehensive Renewable Energy*. vol. 8, A. Sayigh, Ed., ed Oxford: Elsevier, 2012, pp. 111–149.

Horsthemke, J. 2014, Experimentelle Untersuchung einer radialen bidirektionalen Wellenenergieturbine, Bachelor, Institut für Fluid- und Thermodynamik, Universität Siegen, Siegen.

Kentfield, J. a. C. Year, A bi-flow directional air-turbine for wave energy extraction, in *6. International conference on alternative energy sources*, Miami Beach, FL, USA, 1983, pp. 59–60.

Menter, F. R. 1994, Two-equation eddy-viscosity turbulence models for engineering applications, *AIAA Journal,* vol. 32, pp. 1598–1605.

Moisel, C. & Carolus, T. H. 2013, Comparison of axial and radial blade cascades for bi-directional wave energy air-turbines, presented at the 10th European Wave and Tidal Energy Conference (EWTEC), Aalborg, Denmark.

Moisel, C. & Carolus, T. H. Year, Radial lift-based cascade for bi-directional Wave Energy Air-Turbines, in *ASME Turbo Expo 2014*, Düsseldorf, Germany, 2014.

Moisel, C. & Starzmann, R. 2013, Aerodynamic design and numerical investigation of a new radial bi-directinal turbine for wave energy conversion, presented at the 10th European Wave and Tidal Energy Conference (EWTEC), Aalborg, Denmark.

Setoguchi, T. & Takao, M. 2006, Current status of self rectifying air turbines for wave energy conversion, *Energy Conversion and Management,* vol. 47, pp. 2382–2396.

Sigloch, H. 2009, *Technische Fluiddynamik* vol. 7. Dordrecht Heidelberg London New York: Springer Verlag.

Starzmann, R., Moisel, C., Carolus, T., Tease, K. & Arlitt, R. Year, Assessment method of sound radiated by cyclically operating Wells turbines, in *9th European Wave and Tidal Energy Conference*, Southampton, U.K., 2011.